Pergamon

Geochimica et Cosmochimica Acta, Vol. 66, No. 22, pp. 3901–3912, 2002
Copyright © 2002 Elsevier Science Inc.
Printed in the USA. All rights reserved
0016-7037/02 $22.00 + .00

PII S0016-7037(02)00840-2

Pits, outgrowths, and inclusions as coated grain kinetic instabilities

K. TUNCAY[1,1] J. PUCKETT,[2] Z. AL-SHAEIB[2] and P. ORTOLEVA[1,*]

[1]Laboratory for Computational Geodynamics, Chemistry Department, Indiana University, Bloomington, IN 47405, USA
[2]Department of Geology, Oklahoma State University, Stillwater, OK 74075, USA

(*Received August* 31, 2000; *accepted in revised form January* 9, 2001)

Abstract—The development of outgrowths or pits of various shapes on coated grains is explained via a quantitative model of grain growth/dissolution kinetics coupled to evolving grain geometry (morphological dynamics). Grain-coating thinning or fracturing occurring due to nonplanar growth (and consequent grain surface area increase) is shown to underlie an instability to the formation of bumps, or in the case of undersaturated systems, to pitting. Examples of diagenetic outgrowth phenomena on clay-coated quartz are presented. A quantitative model of coupled quartz growth and coating dynamics is shown to imply many features observed in natural systems. Crystal growth anisotropy is shown to strongly influence the morphology of the outgrowths. The creation of inclusions is shown to be closely related to the present morphological instability. These morphological instability phenomena are interesting examples of geochemical self-organization.

A steady-state model of the diffusion of solutes across the grain coating is shown to yield a novel nonlinear equation to be solved for the rate of growth of coated grains. This equation leads to a complex dependence of the growth/dissolution rate on saturation (or more generally on the composition of the fluid) in the medium surrounding the coated grain. The feedback between the dynamics of the coating thickness and morphology changes makes the phenomenon of interest here distinct from that arising from the coupling of grain growth and diffusion in the surrounding medium. This makes pits and needles possible even in a well-stirred surrounding medium, a fact of interest in interpreting the geologic record. For example, the present model can explain the development of spike, mushroom, and other outgrowths on clay-coated quartz grains in a sedimentary rock, whereas the classic Mullins and Sekerke diffusion model cannot, i.e., the time scale for eliminating concentration gradients in a pore is much shorter than that for grain growth. Predictions of the model are consistent with observations on quartz when typical values of diffusion, growth rate coefficients, and other parameters are used. In this paper, we emphasize that pitting can be closely related to outgrowth instabilities. If this be the case, then pitted dissolution of feldspars is a likely example. As feldspars dissolve, they commonly surround themselves with a clay coating, often leaving only a ghost remnant of the original growth. *Copyright © 2002 Elsevier Science Inc.*

1. INTRODUCTION

The growth or dissolution of single crystals in nature is often inhibited by mineral or organic coatings (Heald, 1955). Diffusion through such coatings can be the rate-limiting step, leading to a growth rate that can be orders of magnitude slower than that of a pristine grain. The rate of growth and dissolution can have a complex relation to the saturation (Lasaga, 1981; Anderson and Crerar, 1993); this may be related to surface complex formation or, in the present case, the influence of grain coatings.

In this study, it is shown how the kinetics of coated grains can lead to an implicit growth rate law, i.e., an equation (typically nonlinear) that must be solved for the rate itself. Most interestingly, we show that the state of planar dissolution or growth of coated grains can be unstable to dissolution pitting and needle or other outgrowths.

It is well known that the kinetics of solid growth can support surface morphologic (shape) instability (see Chadam and Ortoleva, 1983, 1986, 1990; Chadam et al., 1987; Ortoleva, 1994, and references therein). However, these models require the diffusion of key components or heat transfer in the growth medium. This classical morphologic instability should be negligible in an aqueous medium within a pore in a rock, as the characteristic growth/diffusion length is much greater than the pore size. However, needle, mushroom, spike, and other outgrowth phenomena are observed in diagenetic systems as seen in Figures 1, 2, and 3. In such a system, $[SiO_2(aq)]$ is essentially uniform in the growth medium (the aqueous pore fluid), in contradiction to the necessary conditions for the classic diffusion-mediated shape instability (Mullins and Sekerka, 1963) noted above. Quartz spikes are relatively common in clay-coated sandstones in the Anadarko Basin (Oklahoma), in the Springer (Mississippian) Sandstone, and in the Spiro (Pennsylvanian) Sandstone of the Arkoma basin.

The objective of this work is to resolve this morphologic paradox by setting forth a mechanism for a grain's growth coupled to the dynamics of its coating and its changing shape. A quantitative model is developed, wherein the growth of a small bump on the grain or minor local thinning of the coating is amplified via a runaway thinning or microfracturing as suggested schematically in Figure 4. The model is implemented for ductile coatings (such as organic amorphous materials or non-brittle clay) and analyzed for morphologic instability. The model is solved numerically to illustrate the growth of large

* Author to whom correspondence should be addressed (ortoleva@indiana.edu).
[1] *Present address:* Faculty of Earth Sciences, Utrecht University, P.O. Box 80021, 3508 TA Utrecht, The Netherlands.

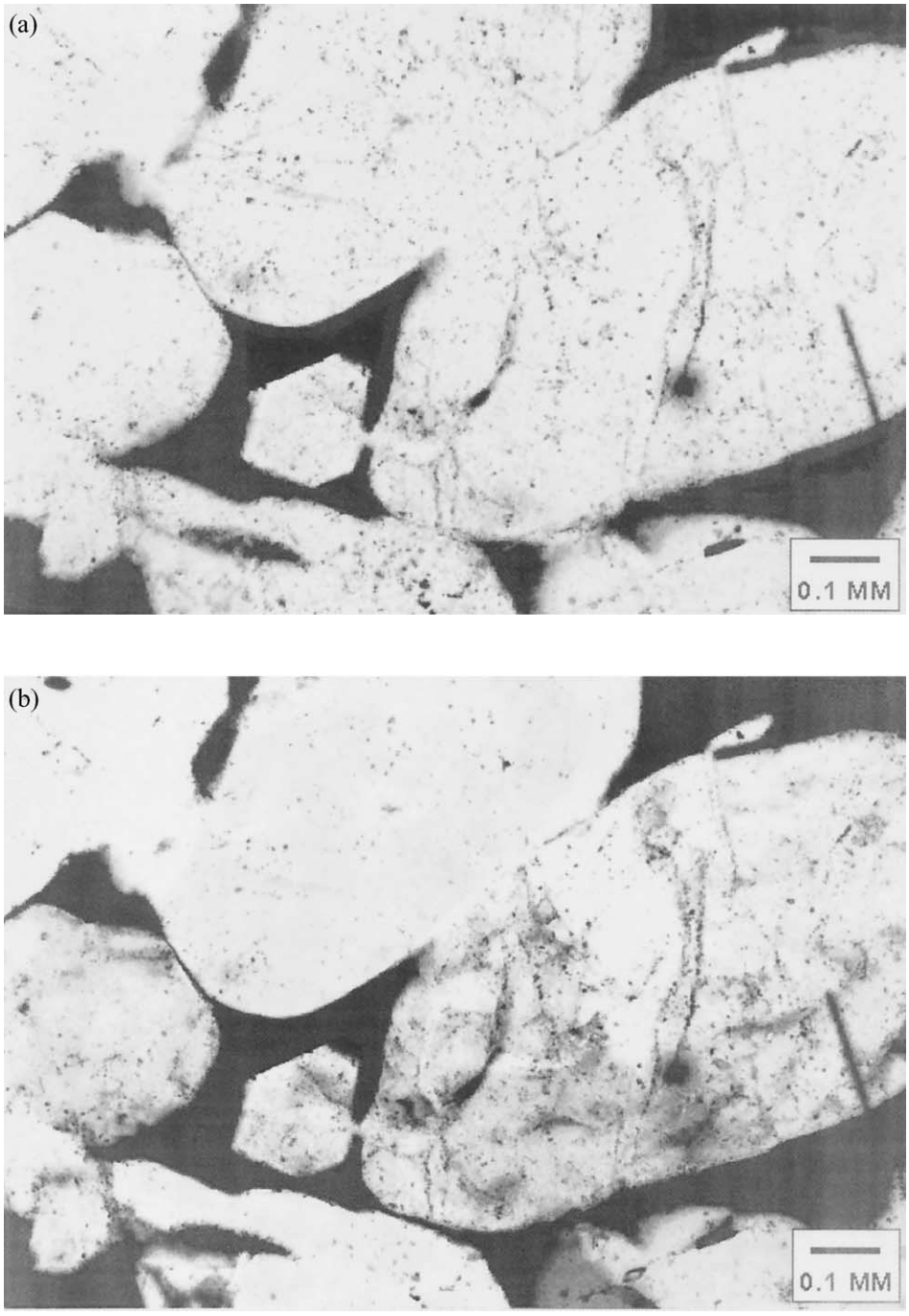

Fig. 1. Plane-polarized light (a) and cross-polarized light (b) pictures of a silica cement "mushroom" that is attached to the quartz host grain by a narrow stem extending through the clay coating that appears as a gray rim in the plane-polarized picture. (Pennsylvanian Spiro Sandstone, Shell Jankowsky well, Arkoma Basin, Oklahoma. Depth is 9814 feet). The mushroom cement displays optical continuity with the host. Quartz overgrowth represents a significant diagenetic stage with drastic effects on primary porosity.

distortions of the grain surface. We investigate the effect of growth-rate dependence on the orientation of the crystal surface relative to the crystallographic axes. The influence of surface free energy, growth kinetics, supersaturation, and average coating thickness on the space and timescale of the phenomenon is identified via a dimensional analysis. Unlike in the case of diffusion-mediated morphologic instability, these phenomena can occur in well-stirred growth media.

Before proceeding, let us clarify the regime in which the specific model presented below is meant to capture. In Fig. 4b we show a breakthrough of a growing protrusion of the underlying grain. When the rate of this bump growth causes exten-

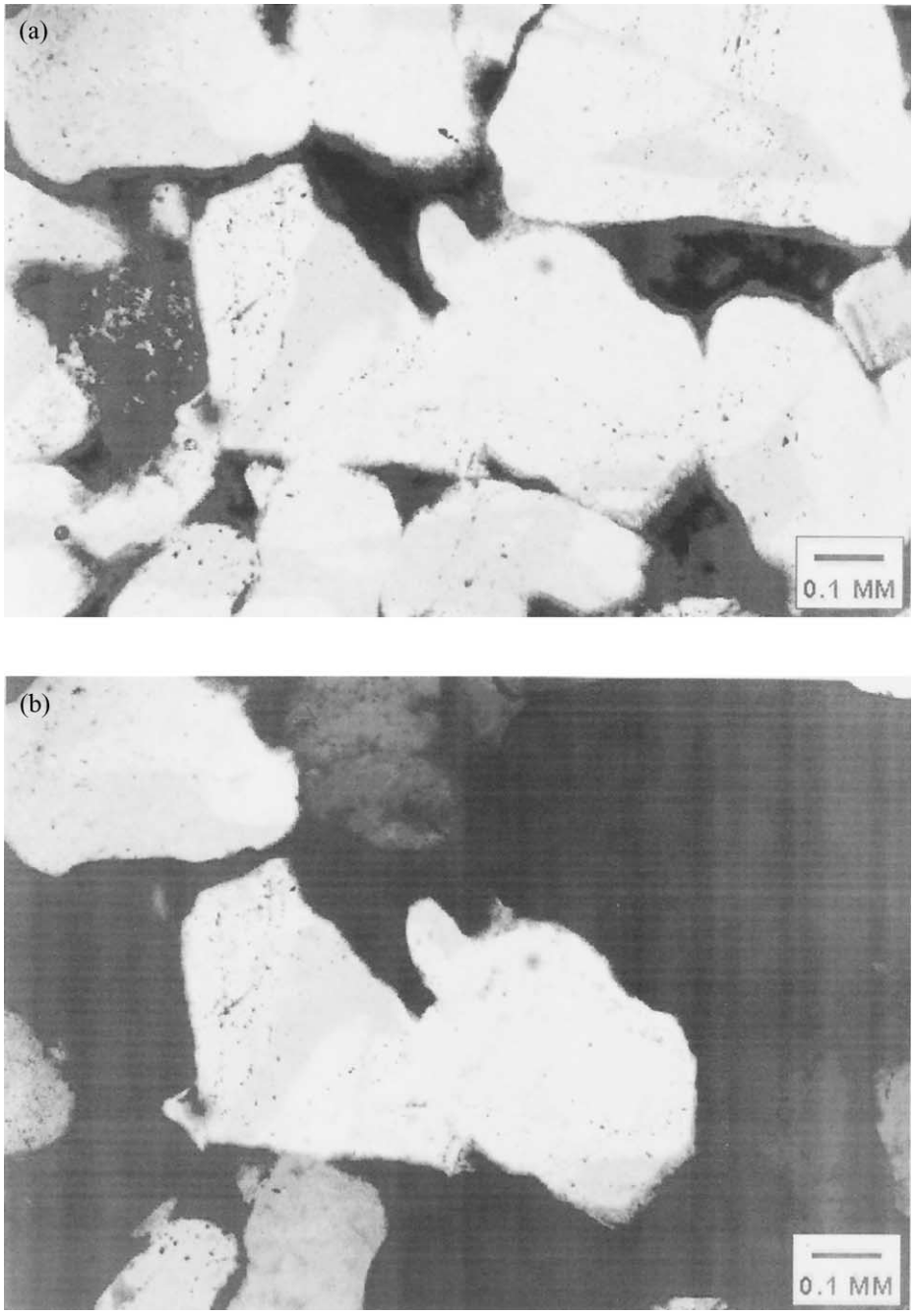

Fig. 2. Plane-polarized (a) and cross-polarized (b) pictures of silica cement in the form of a euhedral quartz crystal "spike" that extends through the clay coating (Shell Jankowsky well, depth 9819 feet). This cement morphology, which has optical continuity with the host, is a rather common feature in clay-coated quartz arenites.

sional stresses in the coating that are beyond a yield point, the coating fails and the growing bump is exposed to the growth medium. The condition for this coating fracturing vs. continuous (viscous) coating thinning/deformation is related to the crystal growth rate, the visco-elastic properties of the coating, and the failure criterion for the latter. In this study, we consider only cases wherein failure does not occur. However, our basic concept of bump amplification, due to augmented growth rate associated with morphology-induced exchange of material between the growing crystal surface and the growth medium, is the same.

The classic Mullins-Sekerke mechanism of grain morphologic instability requires that the timescales for growth and diffusion in the growth medium are comparable. The timescale for the growth of a 1-mm quartz grain is on the year time scale. Diffusion in an aqueous medium in a 1-mm pore is $\sim 10^3$/s (assuming a diffusion coefficient of 10^{-5}cm^2/s). Thus the concentration gradients required for the Mullins and Sekerke

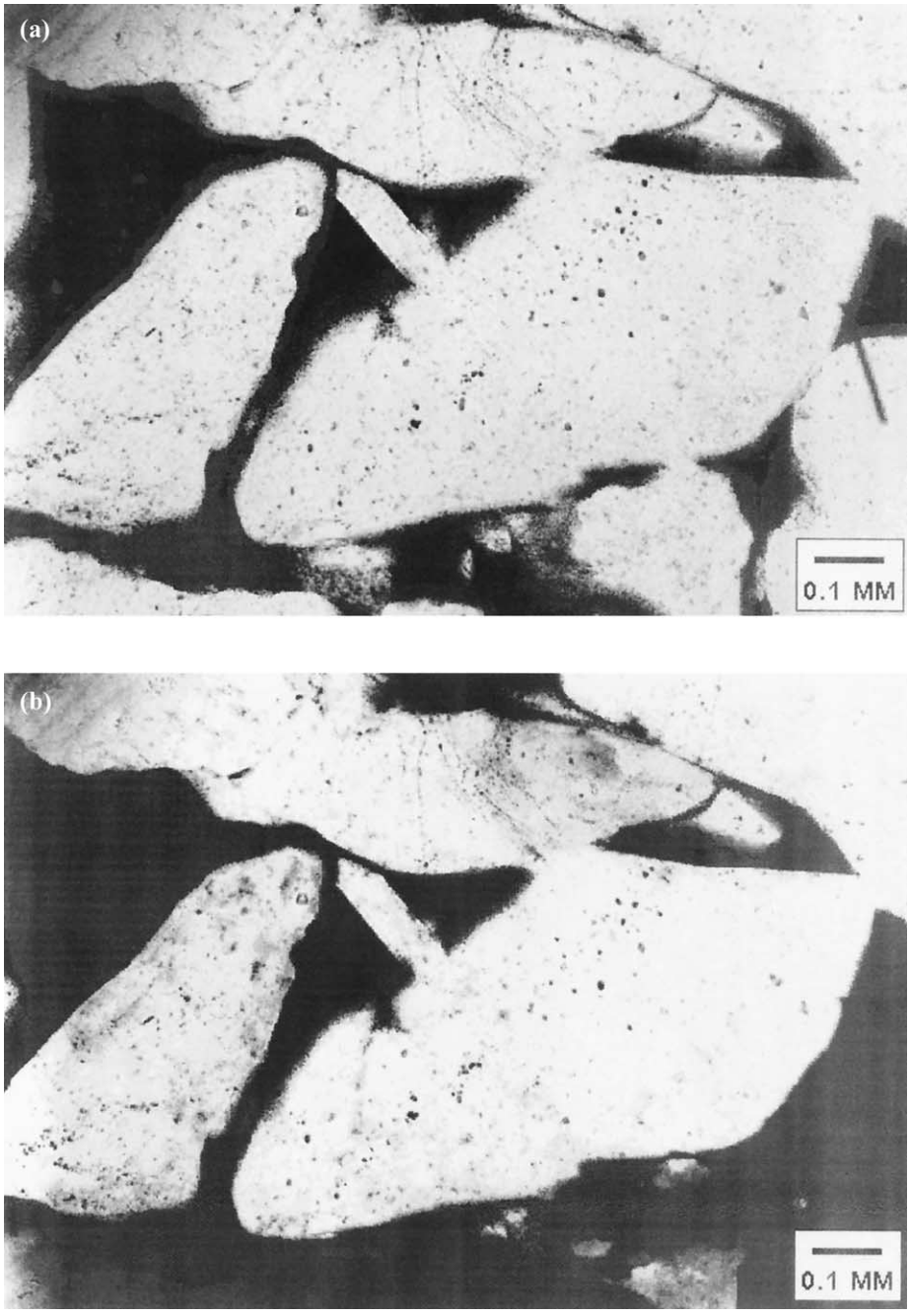

Fig. 3. Plane-polarized (a) and cross-polarized (b) pictures of an oblong, elongate cement extension to a nearly equidimensional quartz grain (Shell Jankowsky well, depth 9819 feet). This feature has optical continuity with the grain and apparently formed beneath the clay envelope, showing that a morphologic instability mechanism involving diffusion through the clay coating is viable.

mechanism cannot explain the features of Figures 1, 2, and 3. As we shall show, the present mechanism can.

2. IMPLICIT GROWTH-RATE LAWS

2.1. Steady-State Formulation

A steady-state diffusion model for coated grain growth/dissolution is now developed. (See Table 1 for a list of symbols used in this paper.) Assume that diffusional mass transfer is the only processes taking place in the coating and that this process is at steady state. Let D_α be the diffusion coefficient of solute species α across the coating. At steady state for a coating of thickness Δ, one has

$$j_\alpha = D_\alpha(c_\alpha - c_\alpha^0)/\Delta, \tag{1}$$

where j_α is the flux of solute α across the coating to the grain

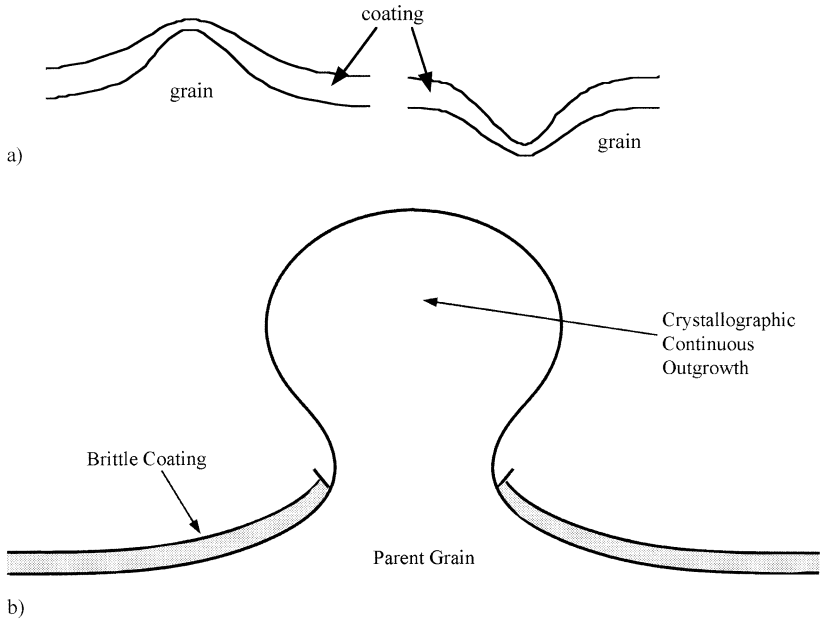

Fig. 4. (a) Incipient needle (left) and pit (right) cause local thinning or microfracturing of the coating. (b) Schematic breakthrough of a grain showing breach of the brittle grain coating.

surface and c_α is the molar concentration of solute α in the fluid beyond the coating (the growth medium) while c_α^0 is the α-concentration at the coating/grain interface. Mass balance at this interface implies

$$j_\alpha = \rho \nu_\alpha G(c^0). \tag{2}$$

Here ρ is the molar density of formula units in the mineral, ν_α is the stoichiometric coefficient for solute α in the grain growth

Table 1. List of Symbols

Symbol	Definition	Units
A	Area	cm^2
c_g	Concentration of solute α in growth medium	mol/L
c_α^0	Concentration of solute α at the grain surface	mol/L
c^{eq}	Saturation value of $[SiO_2(aq)]$ for pristine quartz	mol/L
c^∞	c^{eq} for planar surface	mol/L
D_α	Diffusion coefficient of solute α in coating grains	cm/s
G	Rate of growth of uncoated grain as a function of c^0	cm/s
g	Same as G but thought of as the unknown in (Eqn. 4)	cm/s
j_α	Flux of solute α across the coating	mol/cm^2 s
K	Equilibrium constant in (Eqn. 14)	mol^2/L^2
k	Effective rate coefficient	cm L/s mol
k^0	Rate coefficient for pristine grain	cm L/s mol
N	Number of solute species	none
$\underline{n}$	Unit normal vector to the grain surface	none
$\underline{r}$	Position vector	cm
r^*	Characteristic length	cm
t	Time	s
t^*	Characteristic time	s
u_x, u_z	Growth rate component in x and z directions	cm/s
$\underline{z}$	Unit normal in z direction	none
Δ	Coating thickness	cm
Δ^*	Characteristic coating thickness	cm
δt	Time step in the numerical scheme	s
Γ	A parameter measuring effect of curvature on solubility	cm
κ	Curvature	l/cm
ρ	Molar density of mineral	mol/L
σ	Supersaturation as in (Eqn. 11)	none
$\underline{\tau}$	Unit tangent vector to grain surface	none
ν_α	Stoichiometric coefficient for solute α (see ( ))	none

reaction, and the rate of reaction of the uncoated grain G depends on the c_α^0 (and not on $c = \{c_1, \cdots, c_N\}$) for the N fluid species system. For simplicity, the dependence of G on stress, fluid pressure, and temperature (while important) has not been made explicit (see, however, Ortoleva, 1994).

Our objective is to obtain an equation yielding the rate of growth/dissolution in terms of c (and not c^0). It is now shown that this can only be done implicitly, except for simple cases. Combining Eqn. 1 and 2 yields

$$c_\alpha^0 = c_\alpha - \frac{\rho\Delta\nu_\alpha}{D_\alpha} g. \tag{3}$$

where $g = G(c^0)$. The rate g is yet an unknown function of c. Combining Eqn. 2 and 3 yields

$$g = G\left(\left\{c_\alpha - \frac{\rho\Delta\nu_\alpha}{D_\alpha} g,\ \alpha = 1, \ldots, N\right\}\right). \tag{4}$$

As the functional dependence of G on c_α^0 is presumed known (i.e., from experiments or the theory of the kinetics of uncoated grains), this serves as an equation to be solved for g in terms of c. This is typically a nonlinear algebraic equation that, in most cases, must be solved numerically.

2.2. Growth Anisotropy

A controlling factor on the morphology of growing bumps or pits is the effect of crystal axis orientation relative to the normal n to the crystal surface. To have a semiquantitative model of this phenomenon, assume that the z-axis is the direction of overall growth and is along one of the crystallographic axes. If z is a unit vector in the z-direction, and n is the unit normal to the grain surface, we write

$$u = u_z(\underline{n}\cdot\underline{z})^2 + u_x[1 - (\underline{n}\cdot\underline{z})^2] \tag{5}$$

where u_z and u_x are growth rates when $\underline{n}$ is along the $\underline{z}$ and $\underline{x}$ directions, respectively. We take u_z to be equal to g as obtained above, and u_x is a fixed fraction of u_z. The observations of Figs. 1, 2, and 3 show continuity of crystallographic orientation from the underlying grain into the outgrowth. This suggests that the growth anisotropy of an outgrowth can be directly related to the orientation of crystallographic axes of the underlying grain.

3. ILLUSTRATIVE MINERAL SYSTEMS

The above formulation is now examined for two simple mineral families wherein Eqn. 4 can be solved explicitly.

3.1. Quartz and Other Silica Minerals

Consider the process

$$\text{silica mineral} \rightleftharpoons SiO_2(aq). \tag{6}$$

The free face rate law is often assumed to be

$$G = k^0(c^0 - c^{eq}) \tag{7}$$

where c^{eq} is the saturation value of $[SiO_2(aq)]$. In this case Eqn. 4 reads

$$g = k^0(c^0 - \rho\Delta g/D - c^{eq}). \tag{8}$$

Solving this linear equation for g yields $g = k(c - c^{aq})$ where

$$k = k^0\left(1 + \frac{k^0\rho\Delta}{D}\right)^{-1}. \tag{9}$$

When the Δ is small, the coating-free kinetics is obtained. When Δ is large (i.e., $\Delta \gg D/k^0\rho$), a diffusion-limited kinetic law ($k \to D/\rho\Delta$) is obtained.

A key factor in the phenomenon at hand is surface free energy. This effect mediates against the growth of fine needles, as they are of high free energy and hence are more soluble than morphologies with large radii of curvature. To capture this effect, we adopt the usual assumption that the local free energy, and hence c^{eq}, depends on local curvature $\kappa(\text{cm}^{-1})$. Letting c^∞ be the c^{eq} for a planar surface, we assume

$$c^{eq} = c^\infty(1 + \Gamma\kappa) \tag{10}$$

for parameter $\Gamma(cm)$ that measures the effect of curvature on solubility. For sharp needles, κ is large ($|\Gamma\kappa| > 1$) while for smooth shapes κ is small.

With the above, the rate law can be expressed in terms of supersaturation $\sigma(c^\infty\sigma = c - c^\infty)$ and κ:

$$g = \frac{k^0 c^\infty\sigma}{1 + \Delta/\Delta^*}(1 - r^*\kappa). \tag{11}$$

where $r^* = \Gamma/\sigma$ and $\Delta^* = D/k^0\rho$. Clearly, Δ^* and r^* represent characteristic coating thicknesses and radii of curvature for this system. Furthermore, let $\bar{\Delta}$ be a typical coating thickness for a grain. Then $k^0c^\infty\sigma/(1 + \Delta/\Delta^*)$ is a characteristic growth rate. A natural choice for the characteristic time, denoted t^*, is the typical bump size r^* divided by the characteristic rate and hence

$$t^* = \frac{\Gamma(\Delta^* + \bar{\Delta})}{k^0c^\infty\sigma^2\Delta^*}. \tag{12}$$

In the studies time of section 5, we use units such that Δ^* and r^* are one, while tine units are such that $\Gamma/k^0c^\infty\sigma^2 = 1$. The latter choice was taken because Δ/Δ^* ranges from large values to one or even smaller as the a bump grows and the coating thins locally. The coefficient Γ can be estimated using data on the surface energy (J/cm^2). From the results of Ozkan and Ortoleva (2000) cast for a small spherical grain, one may show that

$$\Gamma = \frac{2(12\pi\bar{v}/N^0)^{2/3}\gamma}{3k_BT(4\pi N^0/3\bar{v})^{1/3}} \tag{13}$$

$\bar{v} = 1/\rho$, γ is the surface energy, N^0 is the Avagadro's number, and k_B is Boltzman's constant. For quartz, γ is $12\mu J/\text{cm}^2$ (Dove, 1995), while $k^0c^\infty \approx 10^{-3}$ cm/yr, $10^{-4} < \sigma < 10^{-2}$, $10^{-12} < D < 10^{-8}$ cm^2/s. Using these values, one finds

$$2.4\ 10^{-8}\ cm < \Delta^* < 2.4\ 10^{-4}\ cm \tag{14}$$

$$5\ 10^{-6}\ cm < r^* < 5\ 10^{-4}\ cm \tag{15}$$

Typical clay coating thicknesses $\bar{\Delta}$ such as in Fig. 3 are 0.005 cm. With the above data ranges and $\sigma = 10^{-3}$ one finds

$$1222 \text{ years} < t^* < 11.6\ 10^6 \text{ years} \tag{16}$$

These characteristic values are consistent with the observations of Figures 1, 2, and 3 and many similar ones we have made on a number of sandstone thermosections.

3.2. Calcite/Siderite/Anhydrite

Consider the group of mineral reactions

$$\text{mineral} \Rightarrow M^Z + A^{-Z}. \tag{17}$$

For mass action kinetics,

$$g = k^0[(c - \eta g)^2 - K] \tag{18}$$

where $\eta = g\Delta/D$, and the concentration of M^Z and A^{-Z} are set equal to c for an assumed stoichiometric mixture, and K is the equilibrium constant. With this,

$$g = \frac{2k^0c\eta + 1 + \sqrt{4k^0c\eta + 1 + 4(k^0)^2\eta^2K}}{2k^0\eta^2}. \tag{19}$$

We have assumed that the diffusion coefficient of M^Z and A^{-Z} in the coating are equal to D. Even in this stoichiometric equal diffusion case, the rate is a complex function of supersaturation σ ($= c^2/K - 1$). For small σ, g is proportional to σ while for large σ (> 0), it goes as c and hence as $\sigma^{1/2}$.

4. NUMERICAL SCHEME

We now present a numerical scheme for simulating the morphologic dynamics of a coated grain. Consider the case of quartz, assuming that D is constant and that the coating has continuous coverage. For simplicity here, we limit our considerations to two-dimensional growth.

The starting point of the numerical approach is the gridding of the grain surface and discretization of time. Let $\underline{r}_i(t)$ be the location of the i-th grid point on the grain surface. A grid point advances from time t to $t + \delta t$ via the time-discretized equation

$$\underline{r}_i(t + \delta t) = \underline{r}_i(t) + \frac{\delta t}{2}[\underline{n}_i(t + \delta t)u_i(t + \delta t) + \underline{n}_i(t)u_i(t)] \tag{20}$$

where u_i is the normal growth rate (G_i/ρ) evaluated at thickness Δ_i and curvature κ_i for the i-th grid point. The second term on the RHS (right-hand side) of Eqn. 20 (and similarly for the developments to follow) are written so as to be second order in δt.

Conservation of coating mass implies

$$\frac{1}{\Delta}\frac{D\Delta}{Dt} = -\frac{1}{A}\frac{DA}{Dt} = -\underline{\tau}\cdot\frac{\partial(u\underline{n})}{\partial l} \tag{21}$$

where τ is a unit tangent vector and A is area. The discretization of Eqn. 21 yields

$$\frac{1}{\Delta_i}\frac{D\Delta_i}{Dt} = -\frac{\underline{r}_{i+1} - \underline{r}_{i-11}}{|r_{i+1} - r_{i-1}|}\cdot\frac{u_{i+1}\underline{n}_{i+1} - u_{i-1}\underline{n}n_{i-1}}{|r_{i+1} - r_i| + |r_i - r_{i-1}|} \tag{22}$$

Grid points $i - 1$, i, and $i + 1$ are transformed to a local coordinate system ξ ($-1 \le \xi \le 1$) and fitted to second order polynomial to calculate the curvature at grid point i. The normal vector n is calculated from the same polynomial.

Our preliminary simulations showed that as morphology changes, the distribution of grid points changes significantly to affect the stability and accuracy of the numerical approach. The inaccuracy results from the curvature and normal vector calculations, as they strongly depend on the local grid resolution and rapidity at which grid spacing changes along the grain surface. We also found that if explicit time-stepping is employed, analogous to diffusion problems, a stability condition ($\delta t < c_1\delta x^{c_2}$) arises. The exponent c_2 is found to be very close to 2. Therefore, when grid points merge due to invagination of the surface, to avoid numerical instability, the time step chosen must be very small. To overcome these difficulties resulting from the uneven distribution of grid points that results as morphology changes significantly, we developed a regridding technique that keeps the distance between the grid points regular after every time step. As a result, grain-coating Δ must be interpolated onto the new grid points. However, care must be made to avoid loss or gain of coating mass due to this interpolation.

Our solution algorithm is as follows:

1. Calculate the normal growth rate using the curvature and grain coating at time t.
2. Calculate the locations of grid points at $t + \delta t$ (via Eqn. 20).
3. Calculate the grain coating at $t + \delta t$ (via Eqn. 22).
4. Calculate the curvature and normal vector using the new grid locations.
5. Calculate the changes in curvature and location of grid points; if error criteria are satisfied, go to step 1 and increase the time step, or else go to step 2 and iterate until error criteria are met. If the number of iterations exceeds a maximum value, decrease the time step and go to step 1.

The tolerances for both locations and curvature between two successive iterations are taken as 10^{-4}. The maximum number of iterations allowed was eight. The time step was increased by 10% and decreased by 50% for successful and unsuccessful time steps, respectively.

5. NUMERICAL SIMULATION RESULTS

The numerical approach presented in the previous section was used to simulate outgrowths in two spatial dimensions. The variables introduced in section 3.1 were used:

$$r^*\tilde{\underline{r}}_i = \underline{r}_i, \qquad t^*\tilde{t} = t, \qquad \Delta^*\tilde{\Delta}_i = \Delta_i. \tag{23}$$

We obtain, dropping the $\sim$, the following problem. The basic equations (Eqn. 20 and 21) with

$$u \rightarrow \frac{1 - \kappa}{1 + \Delta}. \tag{24}$$

In the following set of simulations, we vary key parameters to investigate the behavior of outgrowths on a clay-coated crystal.

5.1. Initially Flat Grain Surface with Locally Thin Coating

The initial conditions are taken with the grain surface at $z = 0$ and $\Delta = 10 - \exp(-(x - 50)^2/4)$ for horizontal axis x. Figure

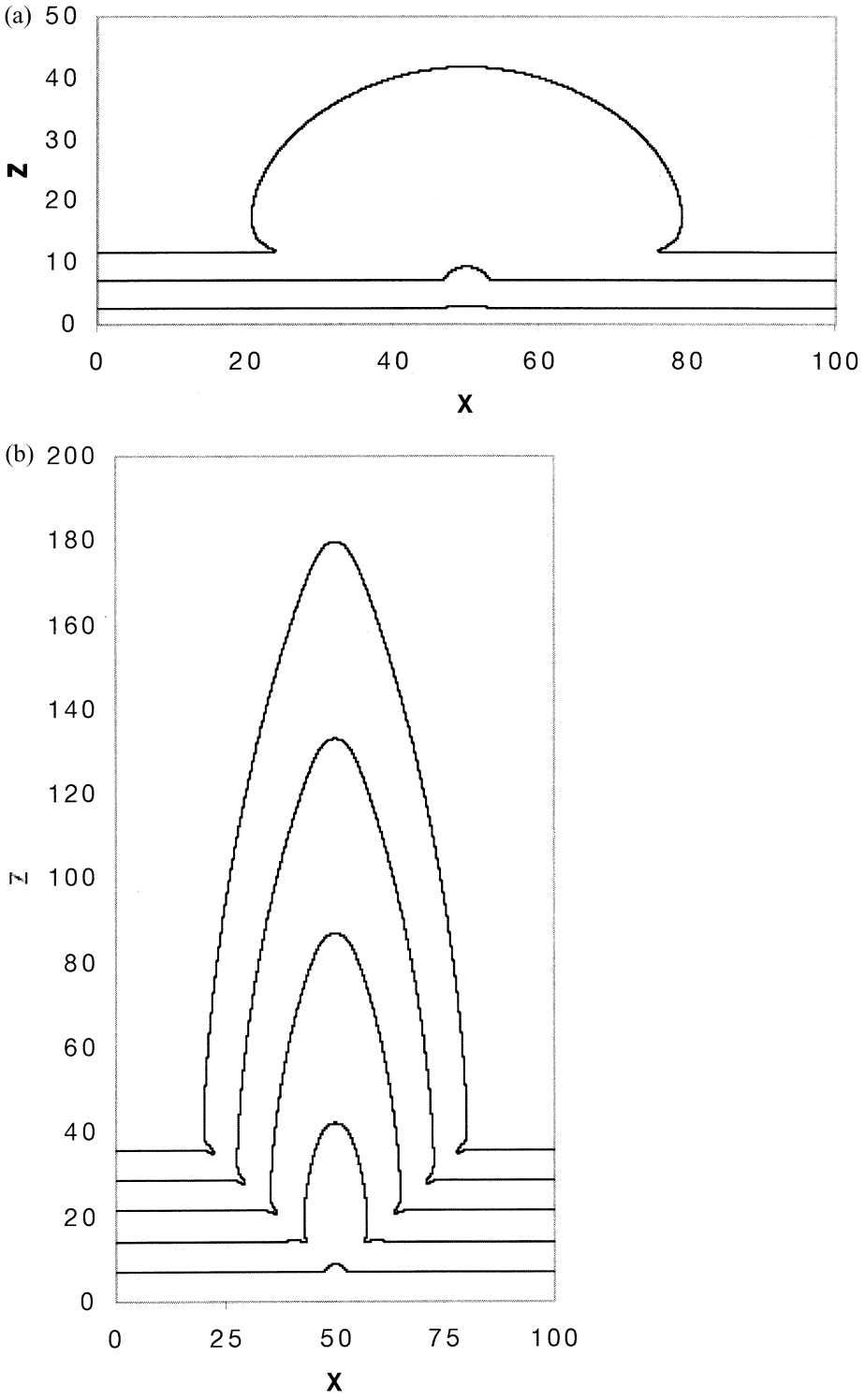

Fig. 5. Evolution of morphology for (a) isotropic (t = 29.73, 79.28, 128.82) and (b) anisotropic (t = 89.19, 168.45, 247.73, 327.01, 406.29) growth scenarios with the initial conditions $z = 0$ and $\Delta = 10 - \exp(-(x - 50)^2/4)$.

5 shows the evolving crystal morphology for isotropic and anisotropic growth. The initially thin coating at the center promotes growth there. Isotropic growth results in an almost circular outgrowth (Fig. 5a), whereas anisotropic growth yields an eccentric bump with an aspect ratio of 3.5. In Figure 6, we see the evolution of an initially slightly thinner (10%) coating at the center for the simulation of Figure 5. Growth increases total grain surface area (length in the present two-dimensional case). The evolving morphology results in a wide region of thin coating and a very narrow region of thick coating for both

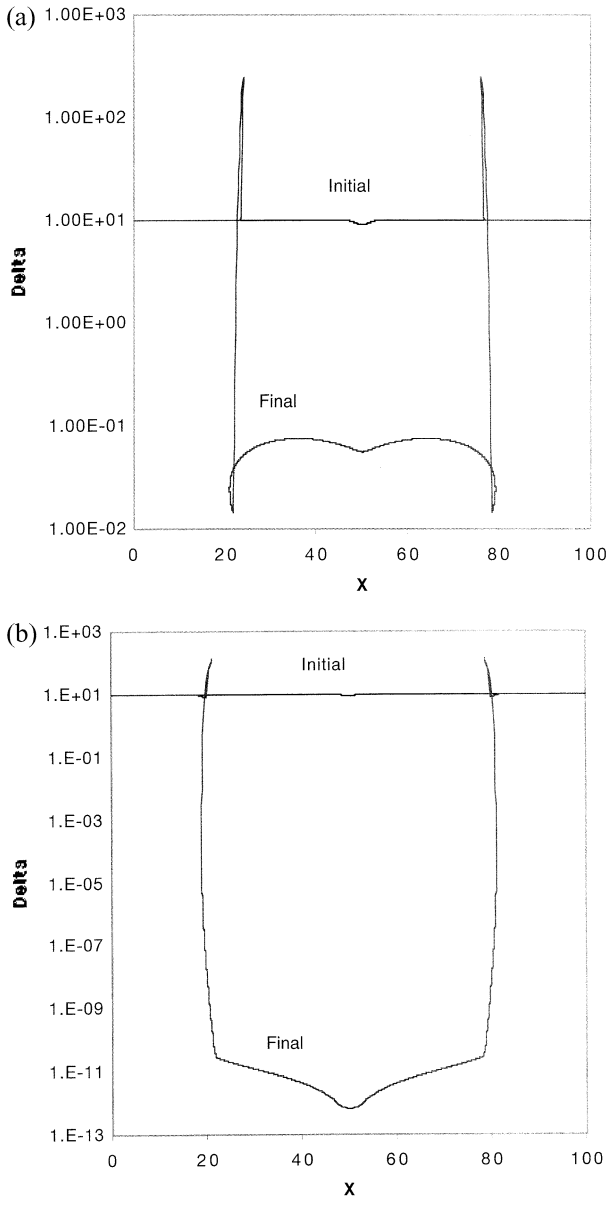

Fig. 6. Evolution of grain-coating thickness for the simulation of Figure 3 for (a) isotropic ($t = 0.00, 128.82$) (b) anisotropic ($t = 0.00, 406.29$) growth scenarios. The multiplicity of Δ as a function of x is related to the bulging in the outgrowth seen in Figure 3.

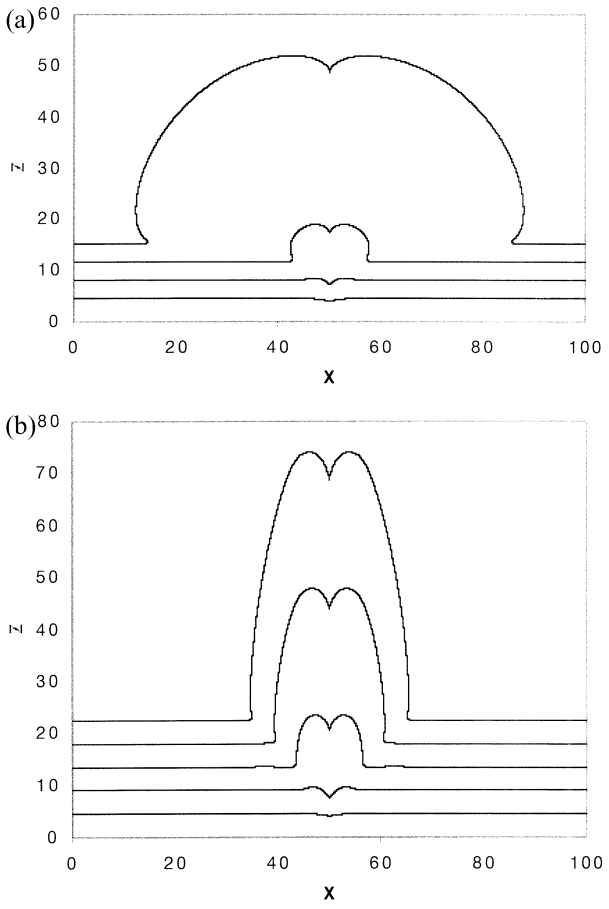

Fig. 7. Evolution of morphology for (a) isotropic ($t = 49.55, 89.19, 128.81, 168.41$) and (b) anisotropic ($t = 49.55, 99.10, 148.63, 198.18$) growth scenarios with the initial conditions $z = 0$ and $\Delta = 10 + \exp(-(x - 50)^2/4)$.

isotropic and anisotropic cases; however, the total mass of grain coating is conserved (i.e., the clay coating is not dissolved or precipitated in the simulation). Our results on grain growth also can be reinterpreted for the case of grain dissolution by putting $u \rightarrow (-1 - \kappa)/(1 + \Delta)$, noting that the equations are symmetric about $z = 0$ and that the equations with $\alpha < 0$ are the same as the growth case but with $t \rightarrow -t$.

5.2. Initially Flat Grain Surface with Locally Thick Coating: Dynamics of Inclusion

The initial conditions are taken with the grain surface at $z = 0$ and $\Delta = 10 + \exp(-(x - 50)^2/4)$. Although the only difference between this case and the previous is the sign in the initial coating disturbance, Figure 7 shows that the resulting morphologies are very different. At early times, the initially thick coating at the center creates a dimple there. A gradual increase in surface area at the sides locally decreases the grain-coating thickness and therefore increases the growth rate there. Meanwhile, the negative curvature at the center increases growth there and thereby competes with the retarding effect of thick grain coating. As in Figure 5a, the isotropic growth rate fosters a circular morphology. Figure 8 shows the results with the grain surface at $z = 0$ and $\Delta = 10 \exp(-(x - 50)^6/4x10^6)$. In this case, there is a broader and thicker local initial disturbance in the grain coating. As the underlying grain grows, it is seen to surround this material and ultimately enclose it to form an inclusion. The shape of the inclusion shown is an early time feature, which over geological time, will tend towards a spherical shape to minimize the surface free energy.

5.3. Initial Bump in the Grain Shape with Uniform Coating

The initial conditions are taken to be $z = \exp(-(x - 50)^2/64)$ and $\Delta = 10$. If $\Delta = 0$, the disturbance in z would be

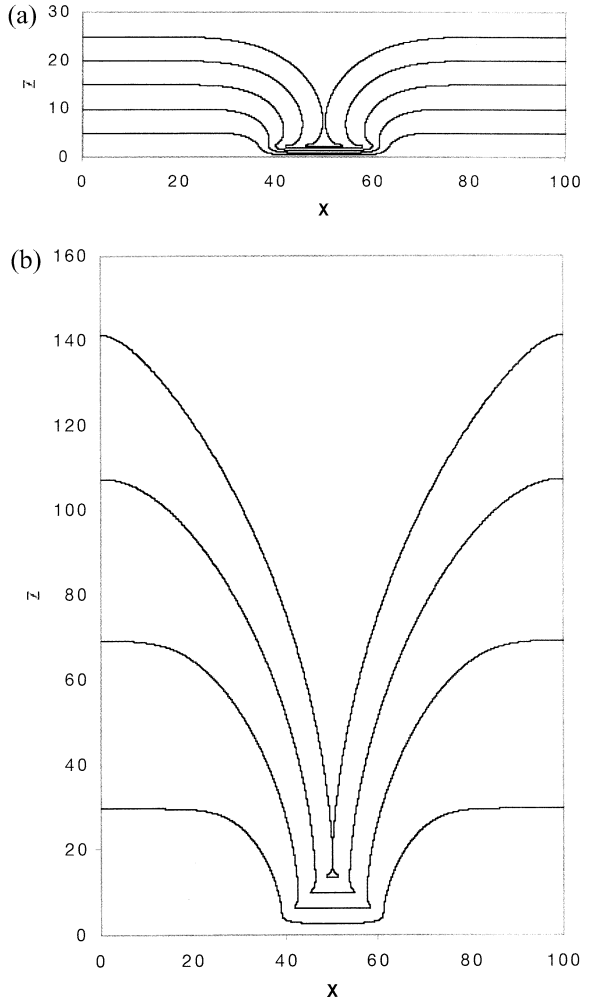

Fig. 8. Evolution of morphology for (a) isotropic (t = 4.97, 9.95, 14.92, 20.92, 24.91) and (b) anisotropic (t = 29.70, 69.34, 108.98, 148.62) growth scenarios with the initial conditions $z = 0$ and $\Delta = 10 \exp(-(x - 50)^6/4x\ 10^6)$.

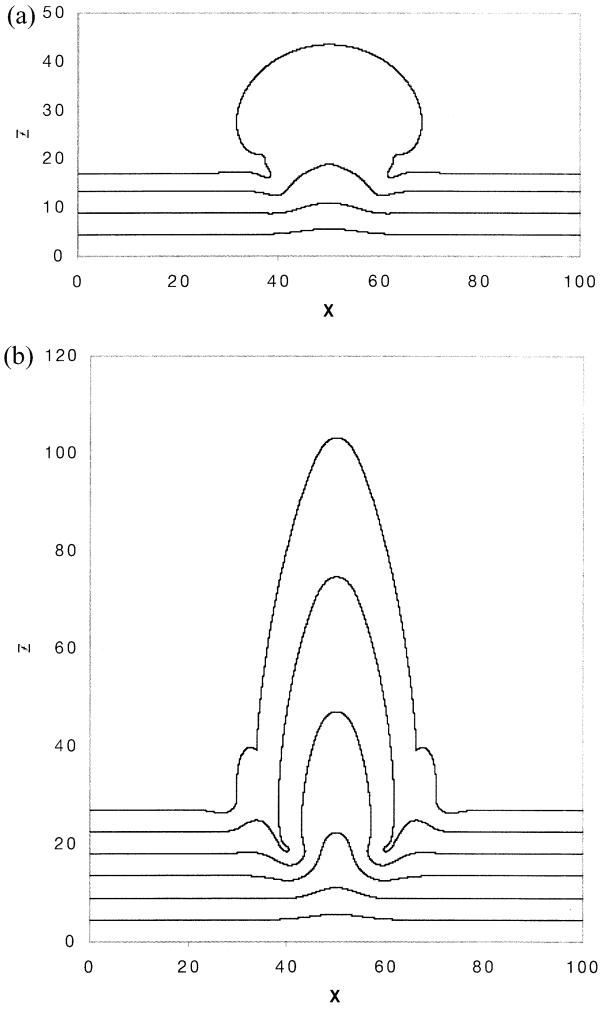

Fig. 9. Evolution of morphology for (a) isotropic (t = 49.55, 99.10, 148.65, 188.29) and (b) anisotropic (t = 49.55, 99.10, 148.64, 198.19, 247.74, 297.28) growth scenarios with the initial conditions $z = \exp(-(x - 50)^2/64)$ and constant grain-coating thickness ($\Delta = 10$).

eliminated by the curvature term in the growth rate. However, the increase in local surface area due to growth at the center thins the grain coating there and eventually increases the local growth rate initiating the morphologic instability (Fig. 9). A "mushroom" is created for the isotropic growth case, whereas in the anisotropic case, an earlier mushroom-like feature transforms into a spike. To study the sensitivity of results on the initial grain-coating thickness, we repeated the simulation except with $\Delta = 1$. As seen in Fig. 10, the resulting morphologies were quite different. As opposed to Figure 9a, Figure 10a shows additional inflection points. Fig. 10b has three peaks of the same height, whereas Figure 9b has one large bump with humps on both flanks. It is also observed that the aspect ratios (height/width) are smaller for both isotropic and anisotropic growth scenarios when the initial coating is thinner. To study the effect of a somewhat different disturbance in the initial condition, we set $z = 0$ for $|x - 50| > 20$, and $z = \exp(-(x - 50)^2/64)$ for $30 < x < 70$ (Fig. 11) and $\Delta = 10$. This corresponds to a sudden (but small) jump in $z \sim 10^{-3}$. Comparisons of Figures 9a and 11a and Figures 9b and 11b show that the additional small disturbance in z eventually affects the morphology of the system.

5.4. Initially Random Grain Surface with Constant Coating

We take $\Delta = 10$ and the initial surface is shown in Figure 12. The short length scale variations in z are eliminated by curvature at an early stage of evolution. This "ripening phase" is followed by a selection process in which larger, lower radius of curvature outgrowths dominate.

6. CONCLUSIONS

The rate of growth/dissolution of coated grains is found as the solution of a nonlinear algebraic equation that yields the dependence of rate on coating properties and growth medium composition. As a result, coated grains exhibit morphologic instability. This addresses the long -standing paradox of how morphologic instability of a growing crystal can occur in the

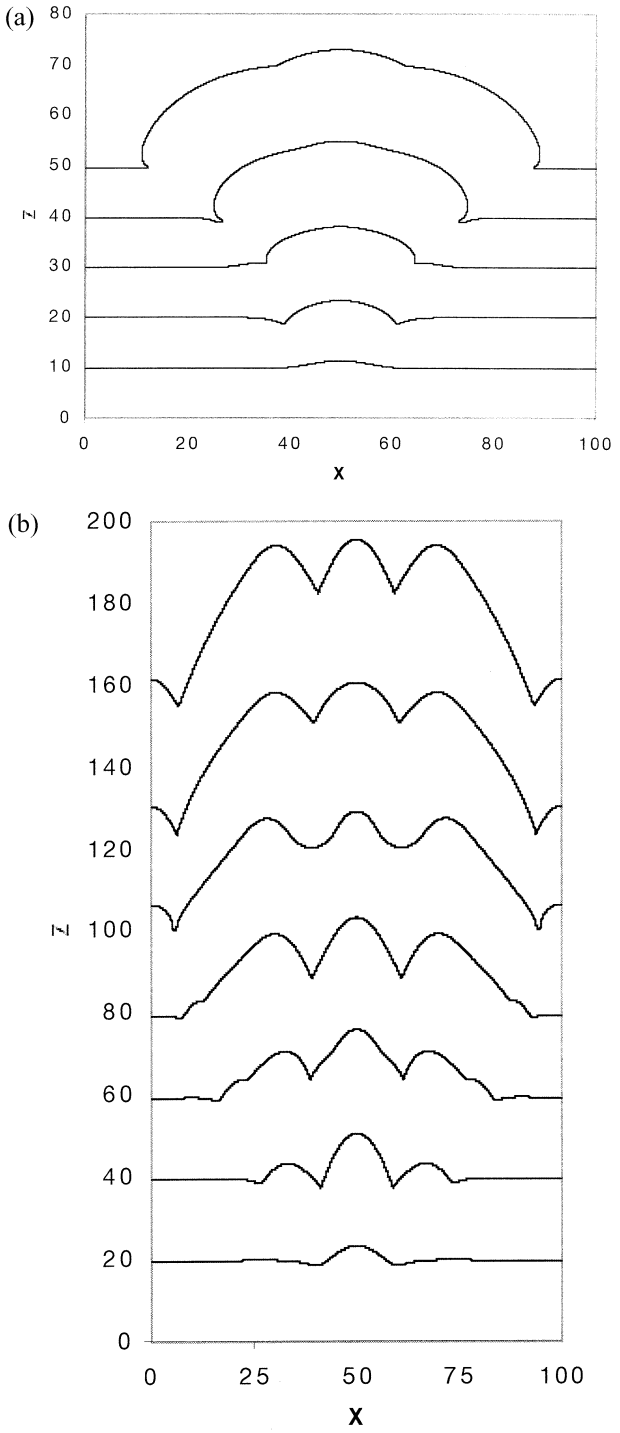

Fig. 10. Evolution of morphology for (a) isotropic (t = 19.82, 49.54, 69.35, 89.16, 108.96) and (b) anisotropic (t = 39.53, 79.25, 118.87, 158.48, 198.12, 237.75, 297.18) growth scenarios with the initial conditions $z = \exp(-(x - 50)^2/64)$ and constant grain-coating thickness ($\Delta = 1$).

absence of gradients of composition or temperature in the growth medium in contrast to the classical model of Mullins and Sekerka (1963, 1964). This instability is manifest during growth and dissolution even if the outside medium is stirred.

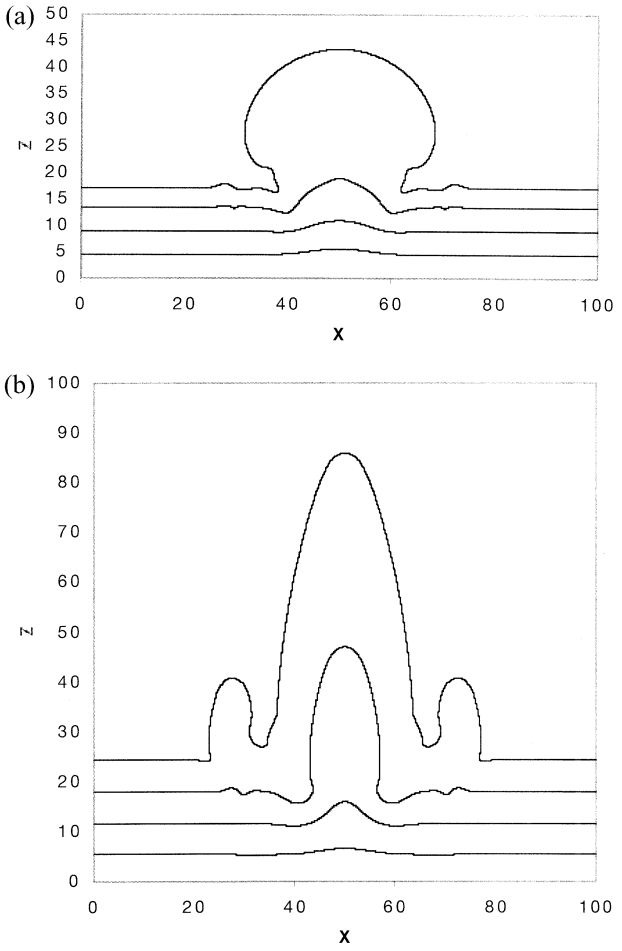

Fig. 11. Evolution of morphology for (a) isotropic (t = 49.55, 99.10, 148.65, 188.29) and (b) anisotropic (t = 59.46, 128.83, 198.19, 267.55) growth scenarios with the initial conditions $z = 0$ for $|x - 50| \leq 20$ and $z = \exp(-(x - 50)^2/64)$ for $30 < x < 70$ and constant grain-coating thickness ($\Delta = 10$).

Simulations of growth coupled to coating dynamics show the formation of bumps, mushrooms, spikes inclusions, and other morphologies, depending on the degree of growth anisotropy and initial coating thickness. The results obtained from the numerical simulations illustrate a tendency to incorporate the coating material as suggested by the coating thickening in the invaginations that develop at the flanks of a growing bump as in Figure 6 or the creation of an inclusion as in Figure 8.

While morphologic instability and large amplitude bumps and mushroom features were obtained, the limits of the physical model prevented extreme morphologies. The most important physical restriction stems from the lack of a physical mechanism to arrest intergrowth.

While the resulting needles and other morphologies are not simply related to the ambient chemical conditions, they are a reflection of it. For example, the characteristic length and time depend on supersaturation, pressure, and through the rate and coating diffusion coefficient, on temperature. Effects such as the finite rate of diffusion across the coating (i.e., breakdown of the steady -state approximation) solid solution (and resulting compositional zoning; see Haase et al., 1980; Ortoleva, 1994)

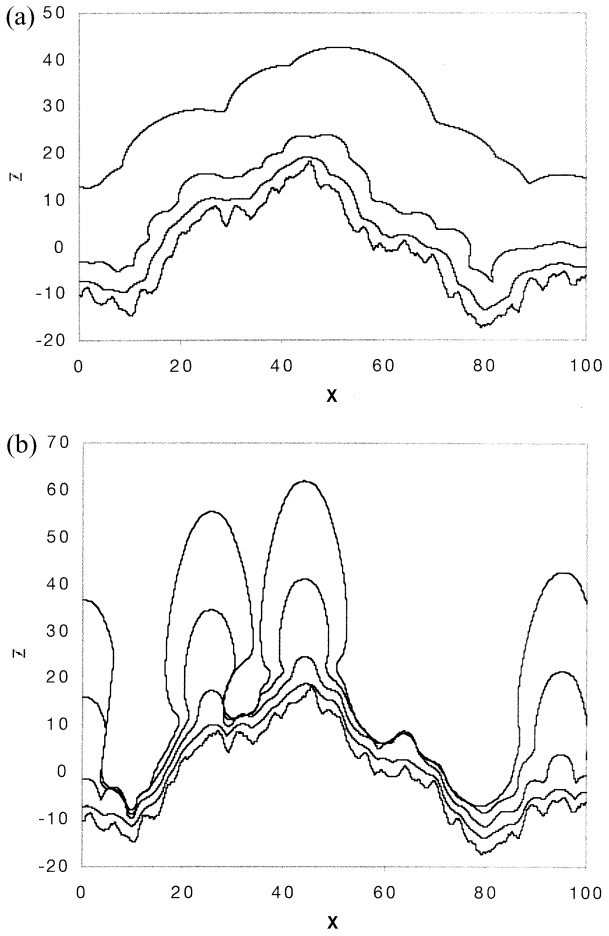

Fig. 12. Evolution of morphology for (a) isotropic (t = 0.00, 29.72, 59.48, 89.16) and (b) anisotropic (t = 0.00, 39.63, 79.26, 118.89, 168.44) growth scenarios with noisy grain topography and constant grain-coating thickness (Δ = 10).

and the effects of coating microfracturing present themselves as interesting directions for the extension of this work. The use of these results in interpreting the geologic conditions accompanying these morphologic instabilities and their use in controlling crystal morphology in manufacturing make these crystal growth phenomenon of practical as well as fundamental interest.

Acknowledgments—We thank Dr. Indu Meshri (Amoco) for pointing out the existence of the needle phenomenon in 1985. We appreciate the support of the GEO/EAR Program of the U.S. National Science Foundation (grant # NSF EAR 99 03132).

Associate editor: J. D. Rimstidt

REFERENCES

Anderson and Crerar (1993) *Thermodynamics in Geochemistry; The Equilibrium Model*. Oxford University Press, New York.

Chadam J., Howison S. D., and Ortoleva P. (1987) Existence and stability for spherical crystals growing in a supersaturated solution. *IMA J. Appl. Math.* **39,** 1–15.

Chadam J. and Ortoleva P. (1983) The stabilizing effect of surface tension on the development of the free boundary in a planar, one-dimensional, Cauchy-Stefan problem. *IMA J. Appl. Math.* **30,** 57–66.

Chadam J. and Ortoleva P. (1986) Moving interfaces and their stability. In *Applications to chemical waves and solidification: Dynamics of Nonlinear Systems* (ed. V Hlavacek), pp. 247–278. Gordon and Breach, New York.

Chadam J. and Ortoleva P. (1990) Reaction-infiltration instabilities. In *Free Boundary Problems: Theory and Applications*, 1 (eds. K. H. Hoffmann and J. Sprekels), pp. 395–404. Longman Scientific and Technical, Harlow, Essex Pitman Research Notes in Mathematics 185.

Dove P. M. (1995) Kinetic and thermodynamic controls on silica reactivity in weathering environments. Chemical weathering rates of silicate minerals. *Rev. Mineral.* **31,** 235–290.

Haase C. S., Chadam J., Feinn D., and Ortoleva P. (1980) Oscillatory zoning in plagioclase feldspar. *Science* **209,** 272–274.

Heald M. T. (1955) Stylolites in sandstones. *J. Geol.* **63,** 10–114.

Lasaga A. C. (1981) Transition state theory. In *Kinetics of Geochemical Processes* (eds. A. C. Lasaga and R. J. Kirkpatrick(eds.; Mineral Society of America, Washington, DC.

Mullins W. W. and Sekerka R. F. (1963) Morphological stability of a particle growing by diffusion or heat flow. *J. Appl. Phys.* **34,** 323–329.

Mullins W. W. and Sekerka R. F. (1964) Stability of a planar interface during solidification of a dilute binary alloy. *J. Appl. Phys.* **35,** 444–451.

Ortoleva P. (1994) *Geochemical Self-Organization*. Oxford University Press, New York.